



Article

Apolar Extracts of St. John's Wort Alleviate the Effects of β -Amyloid Toxicity in Early Alzheimer's Disease

Ahmed El Menuawy^{1,2}, Thomas Brüning¹ , Iván Eiriz¹, Urs Hähnel², Frank Marthe² , Luisa Möhle¹, Anna Maria Górska¹, Irene Santos-García¹, Helle Wangensteen³ , Jingyun Wu¹ and Jens Pahnke^{1,4,5,6,*}

- ¹ Translational Neurodegeneration Research and Neuropathology Lab/Section of Neuropathology Research, Department of Pathology, Medical Faculty/KlinMED, University of Oslo (UiO) and Oslo University Hospital (OUS), Sognsvannsveien 20, 0372 Oslo, Norway
 - ² Institute for Breeding Research on Horticultural Crops, Julius Kühn Institute (JKI)—Federal Research Centre for Cultivated Plants, Erwin-Baur Straße 27, 06484 Quedlinburg, Germany
 - ³ Section for Pharmaceutical Chemistry, Department of Pharmacy, University of Oslo (UiO), Sem Sælands vei 3, 0371 Oslo, Norway
 - ⁴ Institute of Nutritional Medicine (INUM) and Lübeck Institute of Dermatology (LIED), University of Lübeck (UzL) and University Medical Center Schleswig-Holstein (UKSH), Ratzeburger Allee 160, 23538 Lübeck, Germany
 - ⁵ Department of Pharmacology, Faculty of Medicine, University of Latvia, Jelgavas iela 3, 1004 Rīga, Latvia
 - ⁶ Department of Neurobiology, School of Neuroscience, Biochemistry and Biophysics, The Georg S. Wise Faculty of Life Sciences, Tel Aviv University, Tel Aviv 6997801, Israel
- * Correspondence: jens.pahnke@gmail.com; Tel.: +47-23071466

Abstract: *Hypericum perforatum* (St. John's wort) has been described to be beneficial for the treatment of Alzheimer's disease (AD). Different extractions have demonstrated efficiency in mice and humans, esp. extracts with a low hypericin and hyperforin content to reduce side effects such as phototoxicity. In order to systematically elucidate the therapeutic effects of *H. perforatum* extracts with different polarities, APP-transgenic mice were treated with a total ethanol extract (TE), a polar extract obtained from TE, and an apolar supercritical CO₂ (scCO₂) extract. The scCO₂ extract was formulated with silicon dioxide (SiO₂) for better oral application. APP-transgenic mice were treated with several extracts (total, polar, apolar) at different concentrations. We established an early treatment paradigm from the age of 40 days until the age of 80 days, starting before the onset of cerebral β -amyloid (A β) deposition at 45 days of age. Their effects on intracerebral soluble and insoluble A β were analyzed using biochemical analyses. Our study confirms that the scCO₂ *H. perforatum* formulation shows better biological activity against A β -related pathological effects than the TE or polar extracts. Clinically, the treatment resulted in a dose-dependent improvement in food intake with augmentation of the body weight, and, biochemically, it resulted in a significant reduction in both soluble and insoluble A β (−27% and −25%, respectively). We therefore recommend apolar *H. perforatum* extracts for the early oral treatment of patients with mild cognitive impairment or early AD.

Keywords: *Hypericum perforatum*; St. John's wort; Alzheimer's disease; MCI; phytotherapy; silica gel; scCO₂ extract; Syloid[®] XDP3050



Citation: El Menuawy, A.; Brüning, T.; Eiriz, I.; Hähnel, U.; Marthe, F.; Möhle, L.; Górska, A.M.; Santos-García, I.; Wangensteen, H.; Wu, J.; et al. Apolar Extracts of St. John's Wort Alleviate the Effects of β -Amyloid Toxicity in Early Alzheimer's Disease. *Int. J. Mol. Sci.* **2024**, *25*, 1301. <https://doi.org/10.3390/ijms25021301>

Academic Editors: Hari Shanker Sharma and Oxana V. Galzitskaya

Received: 11 December 2023

Revised: 10 January 2024

Accepted: 19 January 2024

Published: 21 January 2024



Copyright: © 2024 by the authors. Licensee MDPI, Basel, Switzerland. This article is an open access article distributed under the terms and conditions of the Creative Commons Attribution (CC BY) license (<https://creativecommons.org/licenses/by/4.0/>).

1. Introduction

Alzheimer's disease (AD) is a progressive neurodegenerative disorder characterized by depression, cognitive decline, memory loss, and functional impairment [1,2]. With the aging population worldwide, the prevalence of AD has been steadily increasing, posing a significant societal and healthcare challenge [3,4].

Amyloid- β (A β) has been shown to play a critical role in AD [5–7]. An elevated concentration of A β in the brain leads to insoluble A β deposits, also denoted as senile or amyloid plaques, resulting in synaptic dysfunction, neuroinflammation, and neuronal loss [8,9]. A β accumulation disrupts regular neuronal signaling pathways and impairs

synaptic plasticity, ultimately causing the cognitive impairment and memory decline observed in the affected individuals [10]. Although A β is not the only biomarker, with TAU, for example, playing a significant role and showing better clinical correlations in patients with disease progression, the role of A β has been reaffirmed by the general effectiveness of monoclonal A β antibodies, despite their problematic side effects [11–13]. This substantiates the *Amyloid Hypothesis* [14,15], which posits A β as the primary trigger for the disease, while not negating the role of other biomarkers and their importance for disease progression and clinical disease severity [16,17], and thereby establishes A β as the main focus of our study.

Despite extensive research efforts, there is little to no effective curative treatment available [18]. The latest FDA-approved, disease-modifying monoclonal anti-A β antibodies (e.g., Adacanumab[®], Lecanemab[®]) demonstrated a significant reduction in A β burden with a clinically minor delay in disease progression [19,20]. More importantly, extreme adverse effects occurred in up to 80.4% of the patients, referred to as A β -related imaging abnormalities (ARIA), including cerebral edema (ARIA-E, up to 30.7%) and cerebral hemorrhages (ARIA-H, up to 30.0%) (meta-analysis of 19 studies in [21]), and, thus, cause substantial concern about its use [19,20,22–24]. Subsequently, the identification of new therapeutic options targeting distinct mechanisms of action is of the highest interest [9,25,26].

ABCC1, also known as multidrug resistance-associated protein 1 (MRP1), belongs to the ATP-binding cassette (ABC) transporter superfamily. It is primarily involved in the efflux of a wide range of endogenous and xenobiotic substances, including glutathione, from cells. Beyond its role in drug resistance, ABCC1 has been implicated in neuroprotection, the modulation of inflammation, and the clearance of neurotoxic substances [27]. Previous research identified ABCC1 induction as a potential mechanism against A β -related, pathological brain effects [28–30].

Hypericum perforatum is a medicinal plant of the *Hypericaceae* family, native to Europe and traditionally widely used as an antidepressant [31,32]. Previous work has also shown the bioactivity of *H. perforatum* extracts with low hyperforin contents in AD model mice, resulting in a reduction of A β in brain tissue [28]. Building upon the findings that *H. perforatum* extracts with low hyperforin content show bioactivity in AD mouse models, leading to a reduction of A β in brain tissue, and demonstrate a hyperforin-independent activation of ABCB1 and ABCC1 transporters [17]—already identified as potential treatment targets for AD [5,14,15,19,22]—other studies have broadened this perspective. These investigations have identified additional compounds within the phloroglucinol group, such as hyperforone, as active substances [33]. Given the multifaceted nature of plant extract effects, which result from the complex interactions between numerous constituents [34], our research adopts a comprehensive approach. We are dedicated to unravelling the intricate details behind these varying results, with the goal of enhancing our understanding and pinpointing the most effective groups of active ingredients. This strategy aims at reconciling conflicting findings and honing in on the specific constituents that hold the most promise for AD treatment.

In addition to ABCC1, the activation of the adenosine triphosphate-binding cassette transport protein P-glycoprotein (ABCB1) has also been observed [35]. *Hypericum perforatum* has been shown to activate at least two transporters [28,35] that play a role in the clearance of toxic molecules from the central nervous system (CNS) [36]. This suggests a multitarget activation of ABC transporters by *H. perforatum*, indicative of its potential broad-spectrum therapeutic impact. The concerted action of these transporters, particularly in the context of neuroprotection and neurotoxic substance clearance, underscores the complex yet promising nature of *H. perforatum* in therapeutic applications.

To further develop effective and controlled AD therapy options based on *H. perforatum*, it is necessary to identify the extracts with optimal activities and reduced side effects. For this purpose, we obtained a total ethanol extract (TE), a polar extract obtained from the TE, and an apolar supercritical CO₂ (scCO₂) formulation, and tested the resulting fractions in an APP-transgenic (APPtg) mouse model. The apolar scCO₂ formulation was

identified as having optimal activity and an adapted treatment paradigm was applied to demonstrate its efficacy to treat A β -related pathology *in vivo*. To further elucidate the chemical composition of the plant extract, detailed analyses were conducted using ¹H Nuclear Magnetic Resonance (NMR) and Heteronuclear Single Quantum Coherence (HSQC) spectroscopy, serving as primary methods for characterizing the extract's molecular constituents [37,38].

2. Results

Due to conflicting statements in the literature, a clear identification of the anti-dementia compounds from *H. perforatum* that work in AD animal models has not yet been achieved.

This study was conducted to clearly delineate active compounds from *H. perforatum* and to identify an effective extract. For this purpose, *H. perforatum* extracts with different polarities were used as an oral treatment in APPTg mice. Appropriate treatment regimens and concentrations were pre-tested and, finally, an early treatment paradigm [39] was employed with a duration of 40 days from 40 days of age. After treatment, protein brain extracts were fractionated to evaluate the treatment's effects on the content of soluble and insoluble A β . Immunoassay determination of A β content from the fractions was then performed to evaluate the treatment efficacy of the herbal extract fractions.

The results showed that one formulation containing the apolar constituents (APOL) particularly resulted in an increase in body weight and increased activity of the animals, in contrast to the control group.

It is important to note that when the dosage of 3.30 mg/gBW was initially administered in the APOL group (protocol in Section 4.4.1.), adverse effects such as weight loss and signs of discomfort were observed (2/8 animals in TE group, 4/8 animals in APOL group). To ensure compliance with animal welfare guidelines, the affected mice were euthanized via cervical dislocation. To address this issue further, a study was conducted in which the full dose was replaced by a three-day dose titration (protocol in Section 4.4.2.). This completely eliminated the adverse effects.

In the final experiment, using dose titration and an adapted early treatment paradigm (protocol in Section 4.4.3.), a significant increase in body weight was again observed in two APOL-treated groups. In addition, one group showed a significant increase in food consumption per mouse. In particular, a reduction in the soluble and insoluble A β 42 fractions in the brain was observed compared to the control group.

2.1. Formulation and Characterization of the APOL Extract

A commercially available supercritical CO₂ extract from *H. perforatum* was chosen to test the apolar extract of *H. perforatum*. The oily and highly viscous properties of the extract presented a challenge for its oral administration via oral gavage. Therefore, a formulation with SiO₂ was employed to overcome this obstacle. The result was a free-flowing yellow powder, suspendable in aqueous phase but not soluble. The powder is satisfactorily homogeneous in particle size, with 84.8% of particles in the range 150–250 μ m in circumference and 82.3% of particles in the range 1000–3000 μ m² in surface area (Figure 1). Inaccuracies in suspension delivery due to excessive differences in particle size are therefore negligible. The right skew of the histograms indicates a quality hurdle in production. It is likely that large particles result from the agglomeration of smaller particles due to cohesive properties of the scCO₂ extract of *H. perforatum* during the manufacturing process. This could be avoided in the future by optimizing the manufacturing parameters. Adaptation of the manufacturing process is important for future industrial applications, but can be neglected for our small-scale study.

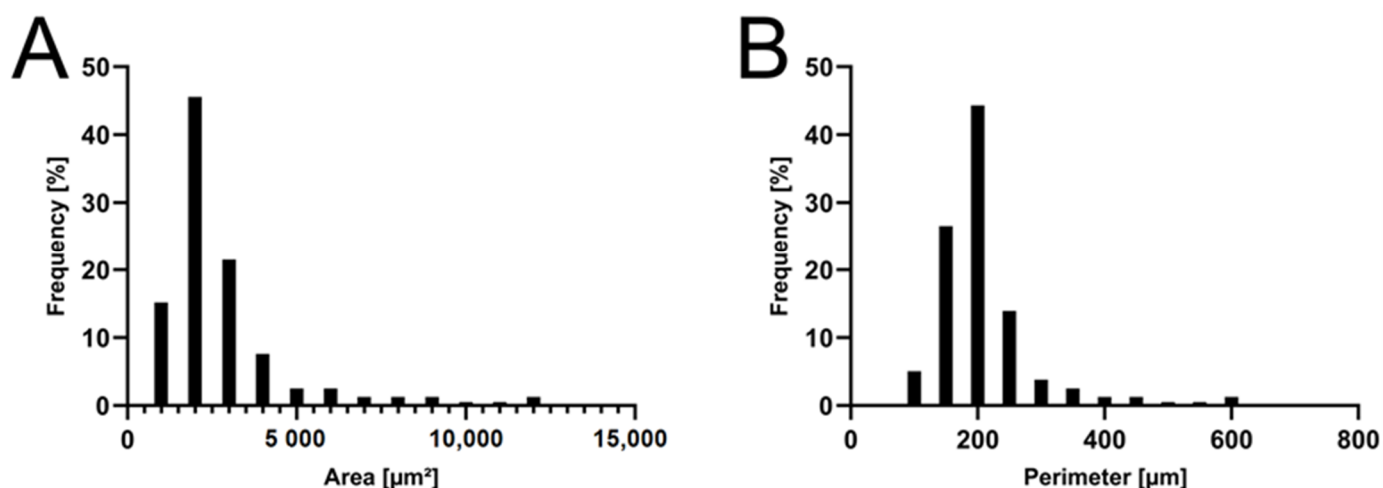


Figure 1. Distribution of APOL particles. Histogram of particle surface area (A) and particle circumference (B) of the APOL batch used. The distribution shows a right skew and thus does not follow a Gaussian normal distribution.

2.2. Toxicity Observations and Treatment Adjustments

Twenty-four hours following the initial oral administration, indications of adverse side effects were detected in the groups subjected to the total extract (“TE”) and CO₂ extract treatments (“APOL”). Within the TE group ($n = 8$), two mice, and in the APOL group ($n = 8$), four mice, displayed adverse effects (apathy). Subsequently, the affected mice were euthanized, enabling symptom-free animals to continue treatment in the subsequent experiment at a reduced dosage without further incidents. Notably, no adverse symptoms were observed in the polar fraction (“POL”) and control groups. These events highlight that unspecified apolar substances, when administered at a high initial dose, as described in Section 2.4.1., can exert a toxic impact on mice.

The supercritical carbon dioxide (scCO₂) extract contains approximately 49.0% hyperforins (Supplementary Material, File S1). Negres et al. [40] reported an LD₅₀ value for hyperforin exceeding 5 mg/gBW, well above our maximum administered APOL dose of 3.3 mg/gBW. Therefore, it is probable that the toxicity arises from other constituents present in APOL or from potential interactions between these constituents. The precise toxic mechanisms associated with APOL require thorough investigation in future research. It is important to note that the observations were confined to the first 24 h following initial dosing. Given the absence of adverse effects such as pain or substantial weight loss (Figure 2), sustained exposure likely led to habituation effects. Consequently, dose titration appears to be the judicious approach.

2.3. Dosage strategy and Optimization

To avoid further adverse effects, dose titration was performed with the three different concentrations listed in Section 4.4.3 to determine a functional APOL dosing scheme. By reducing the initial dose, no adverse events occurred during the first 24 h. Furthermore, no apparent toxic effects were observed when the dose was gradually increased up to 24 h after the maximum dose on day 3.

In subsequent experiments, the dosage was escalated to achieve a maximum daily dosage of 1.8 mg per gram of body weight (mg/gBW) to maximize the desired effects while avoiding observable toxic side effects such as body weight loss. These results offer valuable insights for establishing dosage recommendations in future investigations involving APPTg and APOL.

The best treatment efficiency was commenced starting at 40 days of age, prior to the onset of plaques, for a duration of 40 days (Figure 3). This temporal treatment regi-

men demonstrated the highest efficacy in terms of reducing A β 42 levels, as outlined in Section 2.4.2.

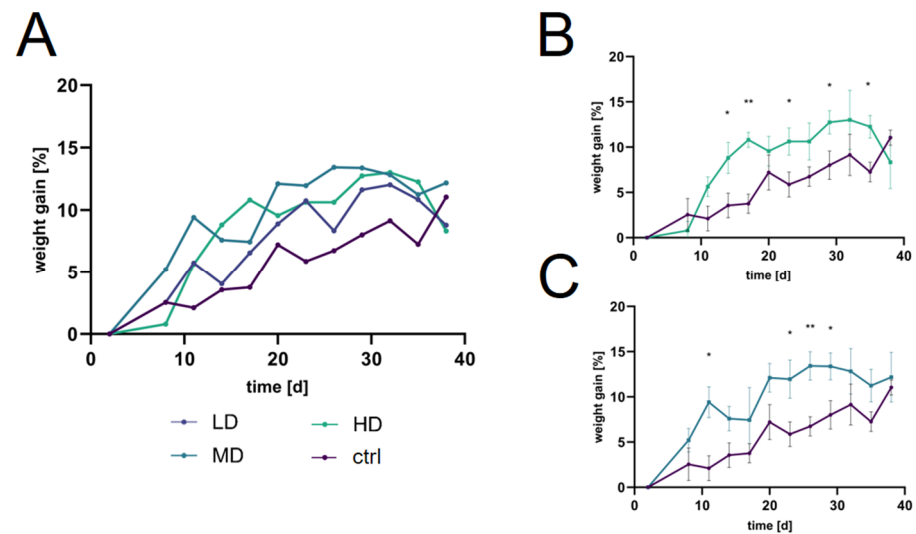


Figure 2. Weight gain of APOL extract-treated mice. (A) Relative increase [%] in body mass of mice treated with APOL over time across three distinct dosage levels. Direct comparisons between ‘HD’ (B) and ‘MD’ (C) treatments versus the control group (ctrl) reveals significant, dose-dependent effects. HD = high dosage, MD = medium dosage, LD = low dosage. Significant differences were assessed using Welch’s *t*-test, * indicates $p < 0.05$, ** $p < 0.01$.

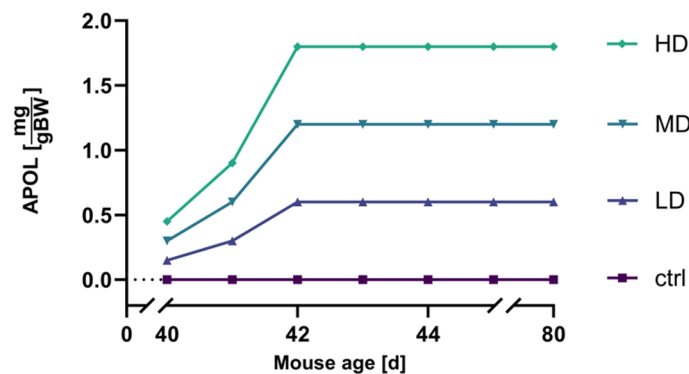


Figure 3. APOL dosage titration. Dosage scheme for three different concentrations of APOL per body weight, during the 40-day treatment period of mice. HD = high dosage, MD = medium dosage, LD = low dosage; control (ctrl) group were treated only with SyloidXDP3050[®].

2.4. Assessment of the Treatment Effects of *H. perforatum* Extracts

2.4.1. Determination of Most Efficient Extract Fraction

To determine which fractions are responsible for the previously reported positive effects in AD treatment, fractions of different polarities were tested against a control group in two repetitions (protocol in Section 4.4.1). First, we detected a significant increase in body weight in the APOL group compared to the controls (Figure 4). No differences between the TE and POL groups and the control group were observed.

However, A β 42 quantification did not reveal any significant differences compared to the control for any of the three extract fractions (Figure 5). Further reduced sample sizes were due to the exclusion of samples that did not meet quality standards during tissue harvesting or protein extraction.

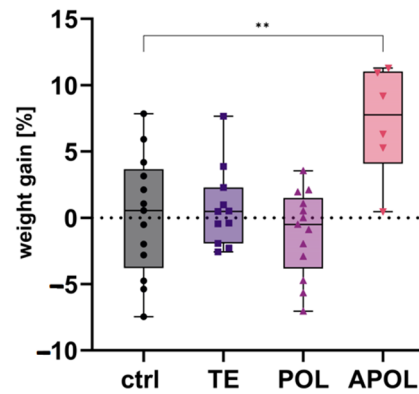


Figure 4. APOL treatment improved body weight. Shown is the relative body weight gain after 25 days of treatment with different fractions of *H. perforatum* (TE = total extract, POL = polar extract, and APOL = scCO₂ extract from SyloidXDP3050®). The control group (ctrl) was treated with tap water. Pooled data of two repetitions are shown as box plots; $n = 6\text{--}13$; significant differences were assessed using Welch's *t*-test, ** indicates $p < 0.01$, the symbols represent individual measurements.

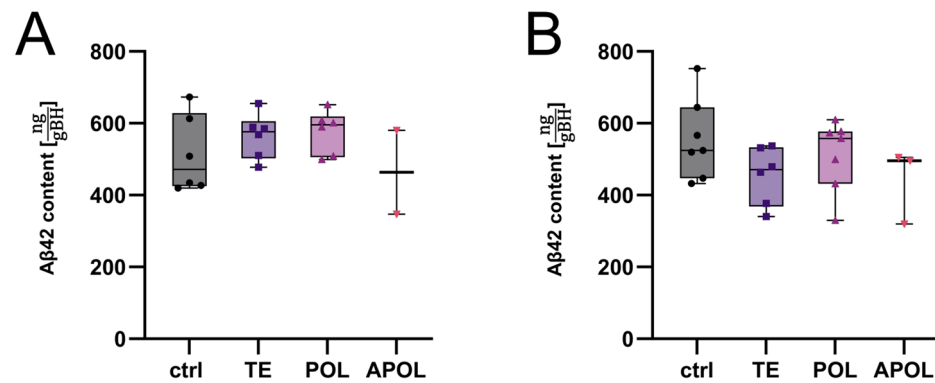


Figure 5. A β 42 content in brain homogenates (BH) of animals treated with different fractions of *H. perforatum* ($n_{\text{final}} = 2\text{--}7$). First (A) and second (B) repetition of A β 42 content quantification via immunoassay in the GuaHCl fraction of brain protein extracts from animals treated with different fractions of *H. perforatum* (TE = total extract, POL = polar extract, and APOL = scCO₂ extract from SyloidXDP3050®). Control group (ctrl) was treated with tap water.

2.4.2. Further Exploration of the APOL Extract

To assess APOL, with the adjusted dosing regimen to prevent adverse effects, three different concentrations of APOL were tested (protocol Section 4.4.3). The findings highlight distinct trajectories for each dosage group (Figure 2A). Initially, the LD group displayed a moderate increase in body weight, which heightened rapidly and plateaued towards the end of treatment. The MD group maintained a steady incline in weight gain, characterized by minor fluctuations throughout the total observation period. The high-dosage (HD) group was particularly noteworthy, starting with a sharp rise, and, while it decelerated slightly over time, the trajectory remained elevated relative to both the LD and MD groups. The significant differences observed in the MD and HD groups, when compared to controls (Figure 2B,C), underscore the treatment-dependent effect on body weight.

The control group exhibited a consistent food intake across the treatment period, with only minor fluctuations (Figure 6A). The LD and MD groups' intake showed slightly elevated intake rates in comparison to the controls, demonstrating minor variances. The HD group presented the most pronounced variation in food intake. The initial phase showed a marked increase in consumption compared to the control group. While there was a transient decline following this surge, intake levels for the HD group remained elevated throughout the study, exceeding that of the controls. However, no significant increase was

found in the HD group due to the high variance, while the LD and MD groups showed a significant elevation of intake over the whole course of the treatment (Figure 6B).

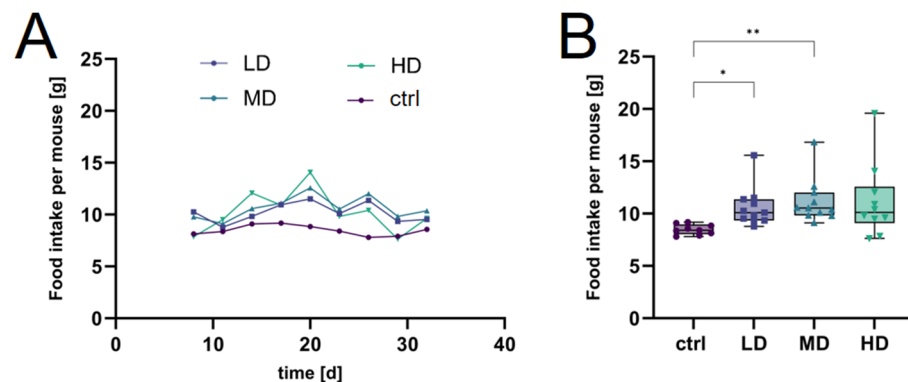


Figure 6. Food intake measurements during treatment. Change in daily food intake per mouse [g] treated with various dosages (LD, MD, and HD) over the treatment period (A) and average overall food consumption per mouse (B). Significant differences were assessed using Welch's *t*-test; * indicates $p < 0.05$, ** $p < 0.01$, the symbols in (B) represent individual measurements.

Determination of A β 42 content using the immunoassay of both protein fractions (GuaHCl and Tris-buffered solution) showed a significantly reduced A β load in the treated groups. A significant reduction in the amount of soluble A β 42 in the TBS fraction per gram of homogenized brain tissue was observed in the LD and HD groups, with an average lower A β 42 content of -26.98% for LD and -25.60% for HD in comparison to the ctrl group (Figure 7A). In the insoluble A β 42 fraction, a significant reduction was observed in the HD group. The mean amount was reduced by -24.90% in the HD group compared to the control group (Figure 7B).

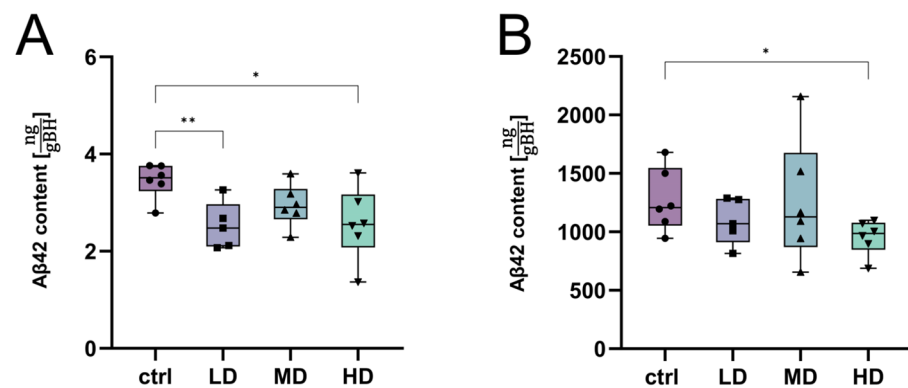


Figure 7. A β 42 content in the soluble and insoluble protein fraction of APOL-treated mice. A β 42 content in the TBS (A) and GuaHCl protein fractions (B) of the brain from APPtg mice treated with APOL at three concentrations (HD = high dosage, MD = medium dosage, LD = low dosage). Controls (ctrls) were treated with SyloidXDP3050[®] only. Data are shown as box plots; $n = 5-7$; significant differences were assessed using Welch's *t*-test; * indicates $p < 0.05$, ** $p < 0.01$, the symbols represent individual measurements.

2.4.3. Characterization of Major Extract Metabolites via NMR Spectroscopy

The ^1H NMR and HSQC spectra of the APOL extract (scCO_2) were dominated by hyperforin signals. This is in accordance with the certificate from the manufacturing company, which stated the a 48.5% presence of hyperforins. There were no signals from flavonoids or hypericin in the NMR spectra of the APOL extract. Characteristic signals from hyperforins are slightly deshielded signals from the methyl groups of the prenyl side chains, giving rise to intense signals in the area $\delta_{\text{H}} 1.5-1.8$, which could be observed in the

HSQC spectrum with corresponding carbon signals at δ_C 18–26. Other prominent signals from hyperforin were the signals from δ_H 4.9–5.2/ δ_C 120–124, corresponding to the olefinic protons of the prenyl groups, methylene groups of the side chains δ_H 1.7–3.2/ δ_C 22–30, and the shielded methyl groups at δ_H 1.0–1.1/ δ_C 14–21 [41].

The 1H NMR spectra of the TE and POL extracts contained the same signals in the aromatic (5.8–8.0 ppm) and carbohydrate regions (3–5.5 ppm) of the spectra. Hyperoside was the major metabolite with characteristic aromatic signals at δ_H 7.83 (d), δ_H 7.58 (dd), δ_H 6.86 (d), δ_H 6.40 (d), and δ 6.20 (d). Epicatechin also demonstrated characteristic signals (e.g., δ_H 6.97 (d), δ_H 5.94 (d), and δ_H 5.91 (d)). We could also observe overlapping signals from other quercetin glycosides (δ_H 7.5–7.8, δ_H 6.8–6.9, and δ_H 6.2–6.4). The major difference between the TE and POL extracts was the absence of hyperforin signals in the POL extract. The prominent methyl signals in the area δ_H 1.5–1.8 in the total extract were totally missing in the POL extract [42,43] (Supplementary Material, File S2, Figures S1–S5).

3. Discussion

Hypericum perforatum is known as an efficient treatment against depression in elderly people, and is widely used in Europe [44]. Specific extracts that have proven their efficiency can also be prescribed by medical doctors and are paid for by national health systems, e.g., as LAIF900[®] in Germany [45,46]. AD- and age-related depression often coincide with dementia or precede the symptoms of depression [1,47,48]. Thus, depression and dementia are two symptoms that are inevitably also connected biologically. It is therefore not surprising that specific plant extracts with anti-depressant characteristics could potentially be used as treatments for AD [30].

During many years of investigations into various plant extracts, we were able to specify lipophilic extracts of *H. perforatum* that possibly have better potential for interfering with dementia symptoms and their biological cause, namely A β deposition [28] or neuronal death [49].

NMR spectroscopy is a powerful technique for the fingerprinting of the major metabolites of herbal extracts, including *H. perforatum* [50]. One of the main advantages with NMR compared to HPLC is that no analysis of standard compounds is needed, as long as reference spectra are available. NMR showed that quercetin glycosides, with the major one being hyperoside, were the dominating aromatic molecules of the total and polar extracts, while hyperforins generated the major signals of the apolar (APOL) CO₂ extract. The total and polar extracts also contained large amounts of carbohydrates. A prominent difference between the total (TE) and polar (POL) extracts was the absence of hyperforin signals in the polar extract.

Having faced technical problems in applying the extracts produced with supercritical CO₂ to mice [28], we decided to solve this problem. The method presented here for formulating highly apolar extracts, such as APOL, with SiO₂, enables their oral application for in vivo experiments with AD mouse models. Nevertheless, there remains room for further optimization of the formulation process, such as a refinement of the production methodology and particle size filtration to achieve a more homogeneous particle size distribution, thereby enhancing the precision in the suspension dosage's administration.

Our initial experiments showed that TE and POL extracts have low to no efficiency in animal experiments at reducing the A β content in brain tissue. The APOL group could not be used to determine any effects of the extract on A β content due to the adverse effects experienced at the dosage we used. Side effects are also often discussed in patient treatment using *H. perforatum* [51]. While weight change is a non-specific parameter influenced by multifactorial aspects, it cannot be used to draw definitive conclusions on its own. However, it has previously been correlated with clinical progression in AD [52–54]. This observation, in conjunction with our ELISA findings (Section 2.4.2), leads us to propose that variations in weight and food intake might represent a secondary beneficial effect in mice. Specifically, weight maintenance or loss at this stage may be indicative of dysfunction, potentially linked to toxic or amyloid-mediated disturbances. Therefore, in the context of our comprehensive

data analysis, the marked increase in body weight and food consumption in mice treated with APOL appears to exert a favorable impact on their overall condition. We observed a significant increase in food consumption after 20 days of the intervention, which finally converges with the control group. This phenomenon might be attributed to the animal's adaptation to the bioactive compounds in the APOL extract, potentially via mechanisms like enhanced metabolism through liver cytochrome enzyme induction [55]. Such adaptation might also elucidate the augmented tolerance towards the extract's toxicity following the initial dosing [56]. To elucidate these observations further, additional studies need to be performed to define the optimal therapeutic setting.

We therefore employed a series of APOL investigations to titrate the toxicity in mice before we continued. In the final experiment, with three adapted APOL dosages, we detected two treatment groups that had significantly increased food intake and body weight. This again allowed for the conclusion that the increased body weight is partly caused by improved feeding behavior. Additionally, we detected a reduction in A β 42 levels in both protein extraction fractions: soluble and insoluble A β , respectively. We therefore concluded that the apolar constituents derived from *H. perforatum* exhibit the best effect to reduce the A β 42 burden in brains of APPtg mice. Former investigations by our group have suggested that this mitigation could potentially be caused by an improvement in the soluble A β clearance facilitated by the activation of ABC transporters, in particular, ABC1 [28,30]. The reduced concentration of soluble A β 42 within the brain of treated mice leads further to a reduction in insoluble A β (aggregates/plaques). Both soluble and insoluble A β contribute to the total toxicity of A β peptides in the brain, and the removal of the soluble A β before touching the insoluble aggregates [9,25,26] might reduce the side effects caused by structural problems in vessels (due to congophil amyloid angiopathy [57,58]) seen in current treatments that use anti-A β antibodies, such as ARIA, ARIA-E, and ARIA-H [21,22].

4. Materials and Methods

4.1. Animal Models and Breeding Scheme

Animal model maintenance and husbandry were performed as previously described [39,59,60]. The individuals used in this study were housed at the Department of Comparative Medicine (section of the Radium Hospital) at the Oslo University Hospital (Oslo, Norway). In this facility, the room macro-environmental parameters included a relative humidity of $62 \pm 5\%$, 15 air changes per hour, an average temperature of 22 ± 1 degree Celsius, and light cycles of 12 h dark/12 h light (strength: 1 lux at night, 70 lux during the day, 400 lux for working illumination). Health monitoring was performed thrice a year according to FELASA guidelines, including opportunists in one of the tests as well. In our experiments, mice were grouped into cohorts of 6–7 individuals in Eurostandard type III cages (Makrolone[®]), provided aspen wood (*Populus tremula*, Tapvei[®], Paekna, Estonia) as bedding substrate, and offered additional enrichment material (tissue paper, tunnel rods, and, occasionally, gnawing sticks). They were fed ad libitum (Rat and Mouse No. 1 Maintenance expanded pellets from SDS, Estonia) and their water was acidified to pH 3 to limit bacterial growth. All experiments were conducted in accordance with the guidelines for animal experiments of the European Union directive and national laws.

The models used in this study were female APPPS1-21 mice [61] (B6.Cg-Tg(Thy1-APPSw,Thy1-PSEN1*L166P)/21JkcrPahnk, APPtg). APPPS1-21 mice have a combined *APP* (Swedish mutations) and *PS1* (L166P mutation) transgene under the control of the *Thy1*-promoter, leading primarily to pathological A β production in the fronto-cortical neurons and their first cortical A β plaques at 45–50 days of age, which also occurs much later in other brain regions as well, but to a significantly lesser extent (e.g., the hippocampus) [29,62].

4.2. Production of Plant Material

Seeds of *H. perforatum* were procured from the seed bank of the Julius-Kühn-Institute (Quedlinburg, Germany). Following germination in a climate chamber at 18 °C for 14 days, they underwent 12 weeks of greenhouse cultivation at 22 °C under artificial illumination

provided by halogen vapor lamps in a short-day rhythm of 10 h daily. The resulting plants were transplanted into a randomized block design, with 10 individual plants per replication. Upon reaching maturity, the inflorescences were harvested and subjected to a three-day drying process in a drying chamber set at 30 °C. To ensure robust results, a composite sample was meticulously created by combining three technical replicates and subsequently utilized for extraction.

4.3. The Extraction and Formulation of *H. perforatum*

Grounded *Hyperici herba* (Ph. Eur. 10.0, 1438 (12/2020)), weighing 200 g, was extracted with 1000 mL of 70% (v/v) ethanol using ultrasound-assisted extraction. The resulting ethanolic extract was taken to dryness by rotary evaporation followed by freeze-drying, resulting in the formation of a solid product with a characteristic purple crystalline appearance. This solid product was labelled as the dried total extract (TE).

The TE was suspended in water and defatted via liquid–liquid extraction, using heptane as the extraction solvent. After removal of the heptane fraction, the resulting aqueous fraction was subjected to the same drying procedures as mentioned above, resulting in the polar fraction (POL), a purple, crystalline, solid mass.

To encompass the apolar substances present in *H. perforatum*, a comprehensive fraction was obtained by procuring a commercially available supercritical CO₂ (scCO₂) extract from FLAVEX Natureextrakte GmbH (Lot nr.: 012501, Rehlingen, Germany).

The scCO₂ extract was first dissolved in heptane, and then silicon dioxide (SiO₂, Syloid® XDP3050, Grace GmbH, Worms, Germany) was added [63–65]. The solvent mixture was subjected to complete evaporation under rotation and vacuum using a rotary evaporator (Hei-VAP Core HL G3B XL, Heidolph Instruments, Schwabach, Germany).

Following the evaporation process, heptane was removed and a yellow free-flowing powder was obtained. This powder exhibited a metastable suspension when introduced into an aqueous solution containing 1.5% methylcellulose. The resulting apolar suspension (APOL) was suitable for oral administration and facilitated the delivery of the scCO₂ extract via oral gavage.

4.4. Treatment Schemes

To evaluate the effects of *H. perforatum* on the APPTg mice, several experiments were conducted, which are elaborated in the following sections. Initially, an assessment was performed using *H. perforatum* extracts of different polarities. Subsequently, an experiment was conducted to optimize the dosing regimen. Following this, a final experiment with an early treatment paradigm was carried out using the most promising dosing scheme, applying three different dosages across three distinct groups.

4.4.1. Treatment Scheme to Test Hypericum Perforatum Extracts (TE, POL, and APOL)

Female mice were first treated with three different extracts of *H. perforatum* via oral gavage for a duration of 25 days (49 to 75 days of age) in three distinct groups of females ($n = 8$) and in two repetitions (Table 1).

Table 1. Treatment scheme for pre-testing of *H. perforatum* extracts. Mouse body weight-adjusted dosage (mg/gBW) for different extracts (TE = total extract, POL = polar extract, and APOL = scCO₂ extract from SyloidXDP3050®). Treatment started at 49 days of age and ended at 75 days of age.

Mouse Age [d]	TE	POL	APOL
49	4.00	4.00	3.30
50	2.00	4.00	1.65
51	2.00	4.00	1.65
52–75	2.00	4.00	1.65

Dried extracts and solid preparations were dissolved in either 1.5% methylcellulose (APOL) or tap water (TE, POL) through stirring for 1–2 h at room temperature (TE, POL) or vortexing for 1 min (APOL). Body weight was recorded weekly throughout the entire duration of treatment. The control groups received tap water. Mice initially received 4.0 mg/gBW TE and POL and 3.3 mg/gBW APOL, respectively. After first dose, the TE and APOL dose was reduced by 50% due to signs of toxicity, resulting in 2.0 mg/gBW for TE and 1.65 mg/gBW for APOL, respectively.

4.4.2. Dosage Titration of the APOL Extract

For further elucidation of the optimal APOL dose titration, two separate groups of female APPTg mice were subjected to a three-day-treatment regimen.

The initial administered dose was set to 0.300 mg/gBW (APOL₁, *n* = 8) and 0.075 mg/gBW (APOL₂, *n* = 8), respectively. Subsequently, a dosage escalation was carried out over the course of the second and third treatment by doubling the dose daily to a maximal dosage of 1.2 mg/gBW and 0.3 mg/gBW across the two delineated groups (Table 2).

Table 2. Treatment scheme for dosage titration [mg/gBW] of APOL extracts (toxicity assessment) over three consecutive days, starting at an age of 49 days.

Mouse Age [d]	APOL ₁	APOL ₂
49	0.300	0.075
50	0.600	0.150
51	1.200	0.300

4.4.3. Early Treatment Paradigm to Assess Efficacy of the APOL Extract Fraction

In the subsequent phase of testing, female mice were treated with three different concentrations (*n* = 7) of APOL via oral gavage in an early treatment paradigm with a duration of 40 days, starting at 40 days of age and continuing until 80 days of age. The suspension was prepared using 1.5% methylcellulose and further vortexed for one minute. The control group received an equally suspended unloaded SyloidXDP3050[®] in 1.5% methylcellulose. Body weight and food intake were recorded in 3-day intervals for the entire duration of treatment (Table 3).

Table 3. Dosage scheme for three different concentrations (mg/gBW) of APOL per body weight, during the 40-day early treatment period of mice (HD = high dosage, MD = medium dosage, LD = low dosage, ctrl = controls treated with SyloidXDP3050[®] only).

Mouse Age [d]	APOL			Ctrl
	HD	MD	LD	
39	0.0	0.0	0.0	0.0
40	0.600	0.150	0.075	0.600
41	0.900	0.300	0.150	0.900
42–80	1.800	0.600	0.300	1.800

4.5. Tissue Harvesting

Mice were euthanized via cervical dislocation. After intracardial perfusion with ice-cold PBS, their brains were removed and separated into two hemispheres. One hemisphere was kept in paraformaldehyde (PFA 4% in PBS, 48 h), the other hemisphere was snap frozen in liquid nitrogen and later transferred to −80 °C until further use.

4.6. Protein Extraction

Frozen hemispheres were thawed on ice in 500 µL RNeasy lysis reagent (Merck KGaA, Darmstadt, Germany) for one hour, removed from liquid and homogenized for 60 s with four

2.8 mm ceramic beads (OMNI International, Atlanta, GA, USA) using a SpeedMill PLUS (Analytik Jena GmbH, Jena, Germany). Twenty milligrams of homogenate was mixed with 10 μ L of cold Tris-buffered saline (TBS, pH 7.5, containing Roche protease inhibitor (VWR, Oslo, Norway)) per 1 mg brain. Samples were homogenized with 2.8 mm ceramic beads (SpeedMill PLUS, 30 s) and centrifuged ($16,000\times g$, 4 $^{\circ}$ C, 20 min) to separate soluble and insoluble A β . The resulting supernatant (TBS fraction containing soluble A β) was collected and stored at -20° C until further use. The pellet was mixed with 8 μ L cold 5 M Guanidine HCl buffer (pH 8.0) per 1 mg brain homogenate, and homogenized (SpeedMill PLUS, 30 s). Samples were incubated at room temperature for 3 h under constant shaking (1500 rpm) before centrifugation ($16,000\times g$, 4 $^{\circ}$ C, 20 min). The supernatant (GuaHCl fraction originally containing insoluble A β) was collected and stored at -20° C until further use.

4.7. Quantification of A β 42

To quantify A β 42 in TBS (soluble) and GuaHCl (insoluble) fractions, we performed electrochemiluminescence immunoassays using the V-PLEX Plus A β 42 Peptide (4G8) Kit and a MESO QuickPlex SQ120 machine, according to manufacturer's recommendations (MesoScale Diagnostics, Rockville, MD, USA) [66–68]. TBS fraction analysis was limited to experiments showing significant differences in A β 42 in GuaHCl fractions.

4.8. NMR Spectroscopy of Extracts

1 H NMR and HSQC spectra were recorded on a Bruker AVNEO400 instrument (Bruker, Rheinstetten, Germany). CD3OD was used as solvent for the total and polar extracts, and CDCl3 was used for the scCO $_2$ extract.

4.9. Statistics

Statistical analysis was performed using Graphpad Prism software (v9, Dotmatics, Boston, MA, USA). We verified the data for Gaussian normal distribution using the Shapiro–Wilk normality test [69]. All data were cleaned of outliers by ROUT (Q = 1%). Welch t-tests were performed to determine the significant differences between two groups. Data are presented as means \pm standard deviation (SD). Differences were considered statistically significant when $p < 0.05$. N is reported in the Figure legends.

5. Conclusions

Our study confirms that the scCO $_2$ *H. perforatum* formulation shows the best biological activity against A β -related pathological effects. Therefore, we recommend apolar *H. perforatum* extracts for the early treatment of mild cognitive impairment or for early AD patients.

Supplementary Materials: The supporting information can be downloaded at <https://www.mdpi.com/article/10.3390/ijms25021301/s1>.

Author Contributions: Conceptualization: A.E.M. and J.P.; methodology: A.E.M., L.M., J.W., I.S.-G., I.E., T.B. and A.M.G.; validation: J.P. and A.E.M.; formal analysis: A.E.M. and H.W.; investigation: A.E.M.; resources: J.P., H.W., F.M. and U.H.; data curation: A.E.M. and J.P.; writing—original draft: A.E.M. and J.P.; writing—review and editing: all; visualization: A.E.M.; supervision: J.P. and H.W.; project administration: J.P. and A.E.M.; funding acquisition: J.P., U.H., F.M. and A.E.M. All authors have read and agreed to the published version of the manuscript.

Funding: A.E.M. received funding from Deutscher Akademischer Austauschdienst/Germany (DAAD, #57556282). A.E.M. and F.M. received funding from Fachagentur für Nachwachsende Rohstoffe (FNR, #22002818 together with Urs Hänel). J.P. received funding from the Deutsche Forschungsgemeinschaft/Germany (DFG, #263024513); Nasjonalforeningen (#16154), HelseSØ/Norway (#2019054, #2019055, #2022046); Barnekreftforeningen (#19008); EEA grant/Norges grants (TAČR, TARIMAD #TO01000078); Norges forskningsrådet/Norway (#295910 NAPI, #327571 PETABC). PETABC is an EU Joint Programme—Neurodegenerative Disease Research (JPND) project. PETABC is supported through the following funding organizations under the aegis of JPND—www.jpnd.eu (NFR #327571—

Norway, FFG #882717—Austria, BMBF #01ED2106—Germany, MSMT #8F21002—Czech Republic, #ES RTD/2020/26—Latvia, ANR #20-JPW2-0002-04—France, SRC #2020-02905—Sweden).

Institutional Review Board Statement: The animal study protocol was approved by the Forsøksdyrutvalget and Mattilsynet (FOTS #7771, 24.06.2015, FOTS #20540, 14.10.2019) for studies involving animals.

Informed Consent Statement: Not applicable.

Data Availability Statement: Data files and Figures can be downloaded from the 'Pahnke Lab-open access' project at DOI: 10.17605/OSF.IO/VWQ58.

Acknowledgments: We would like to thank Anna-Marie Struzek for the fruitful discussions we had with her on the formulation challenges, Beate Helmholtz and Katarina Mehle for their continuous practical support with plant production and processing, Junghanns GmbH (Aschersleben, Germany) for their support with material procurement, and Grace GmbH (Worms, Germany) for providing free samples of their Syloid series silica gel carriers. We also thank the NMR centre of the Department of Pharmacology at the University of Oslo for access to their facilities.

Conflicts of Interest: The authors declare no conflicts of interest.

Abbreviations

A β , amyloid- β ; ABC transporter, ATP-binding cassette transporter; AD, Alzheimer's disease; APP, β -amyloid precursor protein; ARIA, amyloid-related imaging abnormalities; GuaHCl, guanidine hydrochloride; mg/gBW—milligram per gramm of bodyweight; ng/gBH—nanogram per gramm homogenized brain; MW, molecular weight; PBS, phosphate-buffered saline; PFA, paraformaldehyde; SD, standard deviation; SiO₂—silicon dioxide; TBS, TRIS-buffered saline.

References

- Bature, F.; Guinn, B.A.; Pang, D.; Pappas, Y. Signs and symptoms preceding the diagnosis of Alzheimer's disease: A systematic scoping review of literature from 1937 to 2016. *BMJ Open* **2017**, *7*, e015746. [[CrossRef](#)] [[PubMed](#)]
- Wilson, D.M., 3rd; Cookson, M.R.; Van Den Bosch, L.; Zetterberg, H.; Holtzman, D.M.; Dewachter, I. Hallmarks of neurodegenerative diseases. *Cell* **2023**, *186*, 693–714. [[CrossRef](#)] [[PubMed](#)]
- Zhang, X.X.; Tian, Y.; Wang, Z.T.; Ma, Y.H.; Tan, L.; Yu, J.T. The Epidemiology of Alzheimer's Disease Modifiable Risk Factors and Prevention. *J. Prev. Alzheimers Dis.* **2021**, *8*, 313–321. [[CrossRef](#)] [[PubMed](#)]
- Hempel, H.; Prvulovic, D.; Teipel, S.; Jessen, F.; Luckhaus, C.; Frolich, L.; Riepe, M.W.; Dodel, R.; Leyhe, T.; Bertram, L.; et al. The future of Alzheimer's disease: The next 10 years. *Prog. Neurobiol.* **2011**, *95*, 718–728. [[CrossRef](#)] [[PubMed](#)]
- Aisen, P.S.; Vellas, B.; Hempel, H. Moving towards early clinical trials for amyloid-targeted therapy in Alzheimer's disease. *Nat. Rev. Drug Discov.* **2013**, *12*, 324. [[CrossRef](#)] [[PubMed](#)]
- Masters, C.L.; Simms, G.; Weinman, N.A.; Multhaup, G.; McDonald, B.L.; Beyreuther, K. Amyloid plaque core protein in Alzheimer disease and Down syndrome. *Proc. Natl. Acad. Sci. USA* **1985**, *82*, 4245–4249. [[CrossRef](#)]
- Iwatsubo, T.; Irizarry, M.C.; Lewcock, J.W.; Carrillo, M.C. Alzheimer's Targeted Treatments: Focus on Amyloid and Inflammation. *J. Neurosci.* **2023**, *43*, 7894–7898. [[CrossRef](#)]
- Reiss, A.B.; Arain, H.A.; Stecker, M.M.; Siegart, N.M.; Kasselmann, L.J. Amyloid toxicity in Alzheimer's disease. *Rev. Neurosci.* **2018**, *29*, 613–627. [[CrossRef](#)]
- Pahnke, J.; Wolkenhauer, O.; Krohn, M.; Walker, L.C. Clinico-pathologic function of cerebral ABC transporters—implications for the pathogenesis of Alzheimer's disease. *Curr. Alzheimer Res.* **2008**, *5*, 396–405. [[CrossRef](#)]
- Murphy, M.P.; LeVine, H., 3rd. Alzheimer's disease and the amyloid-beta peptide. *J. Alzheimers Dis.* **2010**, *19*, 311–323. [[CrossRef](#)]
- Cummings, J.; Apostolova, L.; Rabinovici, G.D.; Atri, A.; Aisen, P.; Greenberg, S.; Hendrix, S.; Selkoe, D.; Weiner, M.; Petersen, R.C.; et al. Lecanemab: Appropriate Use Recommendations. *J. Prev. Alzheimers Dis.* **2023**, *10*, 362–377. [[CrossRef](#)]
- Budd Haeberlein, S.; O'Gorman, J.; Chiao, P.; Bussiere, T.; von Rosenstiel, P.; Tian, Y.; Zhu, Y.; von Hehn, C.; Gheuens, S.; Skordos, L.; et al. Clinical Development of Aducanumab, an Anti-Abeta Human Monoclonal Antibody Being Investigated for the Treatment of Early Alzheimer's Disease. *J. Prev. Alzheimers Dis.* **2017**, *4*, 255–263. [[CrossRef](#)] [[PubMed](#)]
- Yang, P.; Sun, F. Aducanumab: The first targeted Alzheimer's therapy. *Drug Discov. Ther.* **2021**, *15*, 166–168. [[CrossRef](#)] [[PubMed](#)]
- Hempel, H.; Hardy, J.; Blennow, K.; Chen, C.; Perry, G.; Kim, S.H.; Villemagne, V.L.; Aisen, P.; Vendruscolo, M.; Iwatsubo, T.; et al. The Amyloid-Beta Pathway in Alzheimer's Disease. *Mol. Psychiatry* **2021**, *26*, 5481–5503. [[CrossRef](#)] [[PubMed](#)]
- De-Paula, V.J.; Radanovic, M.; Diniz, B.S.; Forlenza, O.V. Alzheimer's disease. *Subcell. Biochem.* **2012**, *65*, 329–352. [[CrossRef](#)] [[PubMed](#)]

16. Veitch, D.P.; Weiner, M.W.; Aisen, P.S.; Beckett, L.A.; Cairns, N.J.; Green, R.C.; Harvey, D.; Jack, C.R., Jr.; Jagust, W.; Morris, J.C.; et al. Understanding disease progression and improving Alzheimer's disease clinical trials: Recent highlights from the Alzheimer's Disease Neuroimaging Initiative. *Alzheimers Dement.* **2019**, *15*, 106–152. [[CrossRef](#)]
17. Liu, Y.; Tan, L.; Wang, H.F.; Liu, Y.; Hao, X.K.; Tan, C.C.; Jiang, T.; Liu, B.; Zhang, D.Q.; Yu, J.T.; et al. Multiple Effect of APOE Genotype on Clinical and Neuroimaging Biomarkers Across Alzheimer's Disease Spectrum. *Mol. Neurobiol.* **2016**, *53*, 4539–4547. [[CrossRef](#)]
18. Miculas, D.C.; Negru, P.A.; Bungau, S.G.; Behl, T.; Hassan, S.S.U.; Tit, D.M. Pharmacotherapy Evolution in Alzheimer's Disease: Current Framework and Relevant Directions. *Cells* **2022**, *12*, 131. [[CrossRef](#)]
19. Shi, M.; Chu, F.; Zhu, F.; Zhu, J. Impact of Anti-Amyloid-Beta Monoclonal Antibodies on the Pathology and Clinical Profile of Alzheimer's Disease: A Focus on Aducanumab and Lecanemab. *Front. Aging Neurosci.* **2022**, *14*, 870517. [[CrossRef](#)]
20. van Dyck, C.H.; Swanson, C.J.; Aisen, P.; Bateman, R.J.; Chen, C.; Gee, M.; Kanekiyo, M.; Li, D.; Reyderman, L.; Cohen, S.; et al. Lecanemab in Early Alzheimer's Disease. *New Engl. J. Med.* **2023**, *388*, 9–21. [[CrossRef](#)]
21. Jeong, S.Y.; Suh, C.H.; Shim, W.H.; Lim, J.S.; Lee, J.H.; Kim, S.J. Incidence of Amyloid-Related Imaging Abnormalities in Patients with Alzheimer Disease Treated with Anti-Beta-Amyloid Immunotherapy: A Meta-Analysis. *Neurology* **2022**, *99*, e2092–e2101. [[CrossRef](#)] [[PubMed](#)]
22. Sperling, R.A.; Jack, C.R., Jr.; Black, S.E.; Frosch, M.P.; Greenberg, S.M.; Hyman, B.T.; Scheltens, P.; Carrillo, M.C.; Thies, W.; Bednar, M.M.; et al. Amyloid-related imaging abnormalities in amyloid-modifying therapeutic trials: Recommendations from the Alzheimer's Association Research Roundtable Workgroup. *Alzheimers Dement.* **2011**, *7*, 367–385. [[CrossRef](#)]
23. Atwood, C.S.; Perry, G. Playing Russian Roulette with Alzheimer's Disease Patients: Do the Cognitive Benefits of Lecanemab Outweigh the Risk of Edema, Stroke and Encephalitis? *J. Alzheimers Dis.* **2023**, *92*, 799–801. [[CrossRef](#)] [[PubMed](#)]
24. Hegrand, M.; Pahnke, J. [Approval first, research afterwards?]. *Tidsskr. Nor Laegeforen.* **2021**, *141*. [[CrossRef](#)]
25. Pahnke, J.; Langer, O.; Krohn, M. Alzheimer's and ABC transporters—new opportunities for diagnostics and treatment. *Neurobiol. Dis.* **2014**, *72 Pt A*, 54–60. [[CrossRef](#)]
26. Pahnke, J.; Walker, L.C.; Scheffler, K.; Krohn, M. Alzheimer's disease and blood-brain barrier function—Why have anti-beta-amyloid therapies failed to prevent dementia progression? *Neurosci. Biobehav. Rev.* **2009**, *33*, 1099–1108. [[CrossRef](#)] [[PubMed](#)]
27. Cole, S.P. Targeting multidrug resistance protein 1 (MRP1, ABCC1): Past, present, and future. *Annu. Rev. Pharmacol. Toxicol.* **2014**, *54*, 95–117. [[CrossRef](#)]
28. Hofrichter, J.; Krohn, M.; Schumacher, T.; Lange, C.; Feistel, B.; Walbroel, B.; Heinze, H.J.; Crockett, S.; Sharbel, T.F.; Pahnke, J. Reduced Alzheimer's disease pathology by St. John's Wort treatment is independent of hyperforin and facilitated by ABCC1 and microglia activation in mice. *Curr. Alzheimer Res.* **2013**, *10*, 1057–1069. [[CrossRef](#)]
29. Krohn, M.; Lange, C.; Hofrichter, J.; Scheffler, K.; Stenzel, J.; Steffen, J.; Schumacher, T.; Bruning, T.; Plath, A.S.; Alfen, F.; et al. Cerebral amyloid-beta proteostasis is regulated by the membrane transport protein ABCC1 in mice. *J. Clin. Investig.* **2011**, *121*, 3924–3931. [[CrossRef](#)]
30. Pahnke, J.; Frohlich, C.; Paarmann, K.; Krohn, M.; Bogdanovic, N.; Arslan, D.; Winblad, B. Cerebral ABC transporter-common mechanisms may modulate neurodegenerative diseases and depression in elderly subjects. *Arch. Med. Res.* **2014**, *45*, 738–743. [[CrossRef](#)]
31. Ng, Q.X.; Venkatanarayanan, N.; Ho, C.Y. Clinical use of *Hypericum perforatum* (St John's wort) in depression: A meta-analysis. *J. Affect. Disord.* **2017**, *210*, 211–221. [[CrossRef](#)] [[PubMed](#)]
32. Hobbs, C.S. John's wort—Ancient herbal protector. *Pharm. Hist.* **1990**, *32*, 166–169. [[PubMed](#)]
33. Guo, Y.; Huang, F.; Sun, W.; Zhou, Y.; Chen, C.; Qi, C.; Yang, J.; Li, X.N.; Luo, Z.; Zhu, H.; et al. Unprecedented polycyclic polyprenylated acylphloroglucinols with anti-Alzheimer's activity from St. John's wort. *Chem. Sci.* **2021**, *12*, 11438–11446. [[CrossRef](#)] [[PubMed](#)]
34. Wink, M. Modes of Action of Herbal Medicines and Plant Secondary Metabolites. *Medicines* **2015**, *2*, 251–286. [[CrossRef](#)]
35. Brenn, A.; Grube, M.; Jedlitschky, G.; Fischer, A.; Strohmeier, B.; Eiden, M.; Keller, M.; Groschup, M.H.; Vogelgesang, S.S. John's Wort reduces beta-amyloid accumulation in a double transgenic Alzheimer's disease mouse model—role of P-glycoprotein. *Brain Pathol.* **2014**, *24*, 18–24. [[CrossRef](#)]
36. Shen, S.; Zhang, W. ABC transporters and drug efflux at the blood-brain barrier. *Rev. Neurosci.* **2010**, *21*, 29–53. [[CrossRef](#)]
37. Kim, H.K.; Choi, Y.H.; Verpoorte, R. NMR-based metabolomic analysis of plants. *Nat. Protoc.* **2010**, *5*, 536–549. [[CrossRef](#)]
38. Bilia, A.R.; Bergonzi, M.C.; Mazzi, G.; Vincieri, F.F. NMR spectroscopy: A useful tool for characterisation of plant extracts, the case of supercritical CO₂ arnica extract. *J. Pharm. Biomed. Anal.* **2002**, *30*, 321–330. [[CrossRef](#)]
39. Bascunana, P.; Brackhan, M.; Mohle, L.; Wu, J.; Bruning, T.; Eiriz, I.; Jansone, B.; Pahnke, J. Time- and Sex-Dependent Effects of Fingolimod Treatment in a Mouse Model of Alzheimer's Disease. *Biomolecules* **2023**, *13*, 331. [[CrossRef](#)]
40. Negres, S.; Scutari, C.; Ionica, F.E.; Gonciar, V.; Velescu, B.S.; Seremet, O.C.; Zanzfirescu, A.; Zbarcea, C.E.; Stefanescu, E.; Ciobotaru, E.; et al. Influence of hyperforin on the morphology of internal organs and biochemical parameters, in experimental model in mice. *Rom. J. Morphol. Embryol.* **2016**, *57*, 663–673.
41. Lee, J.Y.; Duke, R.K.; Tran, V.H.; Hook, J.M.; Duke, C.C. Hyperforin and its analogues inhibit CYP3A4 enzyme activity. *Phytochemistry* **2006**, *67*, 2550–2560. [[CrossRef](#)] [[PubMed](#)]
42. Tatsis, E.C.; Boeren, S.; Exarchou, V.; Troganis, A.N.; Vervoort, J.; Gerothanassis, I.P. Identification of the major constituents of *Hypericum perforatum* by LC/SPE/NMR and/or LC/MS. *Phytochemistry* **2007**, *68*, 383–393. [[CrossRef](#)] [[PubMed](#)]

43. Rusalepp, L.; Raal, A.; Püssa, T.; Mäeorg, U. Comparison of chemical composition of *Hypericum perforatum* and *H. maculatum* in Estonia. *Biochem. Syst. Ecol.* **2017**, *73*, 41–46. [[CrossRef](#)]
44. Barnes, J.; Anderson, L.A.; Phillipson, J.D. St John's wort (*Hypericum perforatum* L.): A review of its chemistry, pharmacology and clinical properties. *J. Pharm. Pharmacol.* **2001**, *53*, 583–600. [[CrossRef](#)] [[PubMed](#)]
45. Muller, D.; Niederberger, M.; Trenckmann, U.; Volz, H.P. Laif 900 in treatment of depression. Proven reliability in first line therapy. *MMW Fortschr. Med.* **2010**, *152*, 54–55.
46. Uebelhack, R.; Gruenwald, J.; Graubaum, H.J.; Busch, R. Efficacy and tolerability of Hypericum extract STW 3-VI in patients with moderate depression: A double-blind, randomized, placebo-controlled clinical trial. *Adv. Ther.* **2004**, *21*, 265–275. [[CrossRef](#)]
47. Bennett, S.; Thomas, A.J. Depression and dementia: Cause, consequence or coincidence? *Maturitas* **2014**, *79*, 184–190. [[CrossRef](#)]
48. Enache, D.; Winblad, B.; Aarsland, D. Depression in dementia: Epidemiology, mechanisms, and treatment. *Curr. Opin. Psychiatry* **2011**, *24*, 461–472. [[CrossRef](#)]
49. Oliveira, A.I.; Pinho, C.; Sarmiento, B.; Dias, A.C. Neuroprotective Activity of *Hypericum perforatum* and Its Major Components. *Front. Plant Sci.* **2016**, *7*, 1004. [[CrossRef](#)]
50. Rasmussen, B.; Cloarec, O.; Tang, H.; Staerk, D.; Jaroszewski, J.W. Multivariate analysis of integrated and full-resolution 1H-NMR spectral data from complex pharmaceutical preparations: St. John's wort. *Planta Med.* **2006**, *72*, 556–563. [[CrossRef](#)]
51. Brattstrom, A. Long-term effects of St. John's wort (*Hypericum perforatum*) treatment: A 1-year safety study in mild to moderate depression. *Phytomedicine Int. J. Phytother. Phytopharm.* **2009**, *16*, 277–283. [[CrossRef](#)] [[PubMed](#)]
52. Wolf-Klein, G.P.; Silverstone, F.A.; Levy, A.P. Nutritional patterns and weight change in Alzheimer patients. *Int. Psychogeriatr./IPA* **1992**, *4*, 103–118. [[CrossRef](#)] [[PubMed](#)]
53. Du, W.; DiLuca, C.; Growdon, J.H. Weight loss in Alzheimer's disease. *J. Geriatr Psychiatry Neurol* **1993**, *6*, 34–38. [[CrossRef](#)] [[PubMed](#)]
54. Chen, S.; Sarasua, S.M.; Davis, N.J.; DeLuca, J.M.; Thielke, S.M.; Yu, C.E. Weight Loss Is a Strong Predictor of Memory Disorder Independent of Genetic Influences. *Genes* **2023**, *14*, 1563. [[CrossRef](#)] [[PubMed](#)]
55. Madabushi, R.; Frank, B.; Drewelow, B.; Derendorf, H.; Butterweck, V. Hyperforin in St. John's wort drug interactions. *Eur. J. Clin. Pharmacol.* **2006**, *62*, 225–233. [[CrossRef](#)] [[PubMed](#)]
56. Godtel-Armbrust, U.; Metzger, A.; Kroll, U.; Kelber, O.; Wojnowski, L. Variability in PXR-mediated induction of CYP3A4 by commercial preparations and dry extracts of St. John's wort. *Naunyn-Schmiedeberg's Arch. Pharmacol.* **2007**, *375*, 377–382. [[CrossRef](#)]
57. Kuhn, J.; Sharman, T. Cerebral Amyloid Angiopathy. In *StatPearls [Internet]*; StatPearls Publishing: Treasure Island, FL, USA, 2023.
58. Davis, J.; Van Nostrand, W.E. Enhanced pathologic properties of Dutch-type mutant amyloid beta-protein. *Proc. Natl. Acad. Sci. USA* **1996**, *93*, 2996–3000. [[CrossRef](#)]
59. Mohle, L.; Stefan, K.; Bascunana, P.; Brackhan, M.; Bruning, T.; Eiriz, I.; El Menuawy, A.; van Genderen, S.; Santos-Garcia, I.; Gorska, A.M.; et al. ABC Transporter C1 Prevents Dimethyl Fumarate from Targeting Alzheimer's Disease. *Biology* **2023**, *12*, 932. [[CrossRef](#)]
60. Mohle, L.; Brackhan, M.; Bascunana, P.; Pahnke, J. Dimethyl fumarate does not mitigate cognitive decline and beta-amyloidosis in female APPPS1 mice. *Brain Res.* **2021**, *1768*, 147579. [[CrossRef](#)]
61. Radde, R.; Bolmont, T.; Kaeser, S.A.; Coomaraswamy, J.; Lindau, D.; Stoltze, L.; Calhoun, M.E.; Jaggi, F.; Wolburg, H.; Gengler, S.; et al. Abeta42-driven cerebral amyloidosis in transgenic mice reveals early and robust pathology. *EMBO Rep.* **2006**, *7*, 940–946. [[CrossRef](#)]
62. Scheffler, K.; Stenzel, J.; Krohn, M.; Lange, C.; Hofrichter, J.; Schumacher, T.; Bruning, T.; Plath, A.S.; Walker, L.; Pahnke, J. Determination of spatial and temporal distribution of microglia by 230 nm-high-resolution, high-throughput automated analysis reveals different amyloid plaque populations in an APP/PS1 mouse model of Alzheimer's disease. *Curr. Alzheimer Res.* **2011**, *8*, 781–788. [[CrossRef](#)] [[PubMed](#)]
63. Hespeler, D.; El Nomeiri, S.; Kaltenbach, J.; Muller, R.H. Nanoporous smartPearls for dermal application-Identification of optimal silica types and a scalable production process as prerequisites for marketed products. *Beilstein J. Nanotechnol.* **2019**, *10*, 1666–1678. [[CrossRef](#)]
64. Perez-Roman, I.; Kiekens, F.; Cordoba-Diaz, D.; Garcia-Rodriguez, J.J.; Cordoba-Diaz, M. Development of a Solid Formulation Containing a Microemulsion of a Novel Artemisia Extract with Nematocidal Activity for Oral Administration. *Pharmaceutics* **2020**, *12*, 873. [[CrossRef](#)] [[PubMed](#)]
65. Choudhari, Y.; Reddy, U.; Monsuur, F.; Pauly, T.; Hofer, H.; McCarthy, W. Comparative evaluation of porous silica based carriers for lipids and liquid drug formulations. *Open Mater. Sci.* **2014**, *1*, 61–74. [[CrossRef](#)]
66. Griciuc, A.; Federico, A.N.; Natasan, J.; Forte, A.M.; McGinty, D.; Nguyen, H.; Volak, A.; LeRoy, S.; Gandhi, S.; Lerner, E.P.; et al. Gene therapy for Alzheimer's disease targeting CD33 reduces amyloid beta accumulation and neuroinflammation. *Hum. Mol. Genet.* **2020**, *29*, 2920–2935. [[CrossRef](#)]
67. Andrew, R.J.; De Rossi, P.; Nguyen, P.; Kowalski, H.R.; Recupero, A.J.; Guerbet, T.; Krause, S.V.; Rice, R.C.; Laury-Kleintop, L.; Wagner, S.L.; et al. Reduction of the expression of the late-onset Alzheimer's disease (AD) risk-factor BIN1 does not affect amyloid pathology in an AD mouse model. *J. Biol. Chem.* **2019**, *294*, 4477–4487. [[CrossRef](#)]

68. Xia, D.; Lianoglou, S.; Sandmann, T.; Calvert, M.; Suh, J.H.; Thomsen, E.; Dugas, J.; Pizzo, M.E.; DeVos, S.L.; Earr, T.K.; et al. Novel App knock-in mouse model shows key features of amyloid pathology and reveals profound metabolic dysregulation of microglia. *Mol. Neurodegener.* **2022**, *17*, 41. [[CrossRef](#)]
69. Razali, N.M.; Wah, Y.B. Power comparisons of shapiro-wilk, kolmogorov-smirnov, lilliefors and anderson-darling tests. *J. Stat. Model. Anal.* **2011**, *2*, 21–33.

Disclaimer/Publisher's Note: The statements, opinions and data contained in all publications are solely those of the individual author(s) and contributor(s) and not of MDPI and/or the editor(s). MDPI and/or the editor(s) disclaim responsibility for any injury to people or property resulting from any ideas, methods, instructions or products referred to in the content.